RSC Advances

ROYAL SOCIETY OF CHEMISTRY

www.rsc.org/advances

RSC Advances

ARTICLE

Controlled Phosphate Release From Hydroxyapatite Nanoparticles Incorporated into Biodegradable, Soluble host matrixes

Received 00th January 20xx,
Accepted 00th January 20xx

DOI: 10.1039/x0xx00000x

www.rsc.org/

A. S. Giroto,[a,b] S. C. Fidélis[a,b] and C. Ribeiro[b*]

We report in this paper a strategy to prepare nanocomposite fertilizers based on the dispersion of hydroxyapatite (Hap) into urea and thermoplastic starch at nanoscale, where Hap was assumed as a model for poorly soluble phosphate phases, such as phosphate rocks. Our experiments revealed the role of particle agglomeration on the effective phosphate release, showing that Hap dispersion within two water-soluble matrices (urea and thermoplastic starch/urea) is an effective strategy to increase Hap solubility. Aspects such as matrix solubility, morphology and Hap loading were detailed studied. Also, these structures showed an interesting slow-release of urea, i.e., the materials were at the same time a system for faster release of poorly soluble phosphate phases and slow release of very soluble nitrogen source (urea). Our results support the development of a new class of smart fertilizers, with release properties tailored by nanostructure.

Introduction

Fertilizers supply is one of the key aspects of high productivity in agriculture, chiefly for the macronutrients nitrogen (N), phosphorus (P) and potassium (K). Phosphorus is the least element required by plants, however this nutrient has limited the agricultural production due to its low availability in soils, especially in tropical areas.[1] Unfortunately, the low solubility of phosphate rocks limits their direct application as a fertilizer. As a consequence, phosphate rocks have been converted into soluble phosphate fertilizers by using chemical means.[2] An alternative to this issue would be increasing the solubility of phosphate minerals by the aid of nanotechnology. This technology has been proposed as an emerging approach with enormous potential to improve the effectiveness of agricultural fertilizer.[3] Due to the very small size and high surface to volume ratio, nanoparticles are expected to dissolve faster than their bulk counterparts.[4,5] The distinctive properties of nanoparticles could be used to design more efficient P fertilizers as well.[6] Some works have showed that the reduction of the particle size of soluble phosphate rocks improves their agronomic effectiveness[7] because of the increase in the dissolution rate and higher probability of the nanoparticles to interact with the roots.[8,9] This concept was also recently used by Montalvo et al.[10] who evaluated the use of hydroxyapatite nanoparticles as a potential P-fertilizer with improved efficiency based on the hypothesis that nano-sized particles can diffuse more easily through the soil to reach the plants. The dispersion of P-fertilizers within organic matrices could also be combined with the particle size reduction approach as well as techniques that avoid particle re-agglomeration. Recently, Liu and Lal[11] investigated the use of hydroxyapatite nanoparticles (15 nm) dispersed into carboxymethyl cellulose as a novel P-fertilizer which exhibited enhanced efficiency and lower eutrophication risk than conventional water-soluble calcium phosphate. Therefore the organic matrix could also serve as an electrostatic barrier to hinder the fixation of phosphate nanoparticles in soil, principally in those with higher contents of humic acid as reported by Wang et al.[12]

Organic matrices used in the formation of nanocomposites must necessarily be compatible with the hydrophilic surface of the phosphate nanoparticles, and it is also desirable that the matrix/phosphate nanoparticles formulation could be continuously processed, e.g. by extrusion. Two interesting candidates to be used as a matrix are urea and thermoplastic starch. Urea is a water soluble compound and the main N-fertilizer used for agricultural crops, while thermoplastic starch has lower solubility and has been extensively studied as a polymer matrix of nanocomposites due to its renewable, biodegradable, plentiful and inexpensive aspects.

Hence, the objective of this work was to examine the solubility in water of nano-scaled inorganic phosphate particles and their interactions with matrices of different solubility: urea and thermoplastic starch (TPS). This works further describes how the release process of PO_4^{3-} ions can be tailored by nanocomposite production strategies. The use of nanocomposites could support the further development of a new class of smart fertilizers, which will permit new applications for poorly soluble phosphate mineral phases.

[a] Federal University of São Carlos, Department of Chemistry - Washington Luiz Highway, km 235, São Carlos - SP, Zip Code: 13565-905, Brazil.
[b] Embrapa Instrumentation, 1452 XV de Novembro Street, São Carlos - SP, Zip code:13560-970, Brazil.Email:caue.ribeiro@embrapa.br Tel/fax:+55162107-2915/2903

Experimental section

Materials

The raw materials used in the nanocomposite formulations were:urea (Synth, Diadema, SP, Brazil), hydroxyapatite (Sigma-Aldrich, St. Louis, MO, USA), Amidex 3001 (Corn Products, Sao Paulo, SP, Brazil) citric acid (Synth, Diadema, SP, Brazil), and stearic acid (Vetec, Duque de Caxias, RJ, Brazil). All the other materials were used as received.

Preparation of Nanocomposites

Ur/Hap

The nanocomposites were prepared by mixing urea (Ur) and hydroxyapatite (Hap) at different urea/Hap ratios ($w.w^{-1}$ basis) of 1:1 (50% Hap), 2:1 (33% Hap), and 4:1 (20% Hap) according to the procedure reported by Pereira et al.[13] varying the extrusion temperature close to the urea melting range. The nanocomposite samples were produced using a torque rheometer (Polylab RHEODRIVE Rheomix mixer and OS4) under the conditions of 60rpm for 10min at 100°C. The materials were dried at room temperature for 24 hours. The nanocomposites were designated as Ur/Hap 1:1, Ur/Hap 2:1, Ur/Hap 4:1 with respect to the urea/Hap mass ratio, respectively.

TPS:Ur/Hap

The thermoplastic starch (TPS) was obtained by a physical mixture of corn starch, urea (Ur) and distilled water at a mass proportion of 56/24/20, respectively. To this blend we added 1% ($w.w^{-1}$) of stearic acid and 1% ($w.w^{-1}$) of citric acid. This final TPS:Ur formulation was processed in a co-rotating double screw extruder (L/D = 40, ZSK-18 Coperion model) equipped with driving and mixing elements. The extruded was setup with 6 heating zones at temperatures of 100, 110, 115, 120 at 130°C to 120°C, and rotating speed of 150 rpm to obtain TPS:Ur blends in the form of pellets. The TPS:Ur/Hap nanocomposites with Hap mass contents of 50, 30 and 20% were synthesized by premixing and processing the powders (starch, urea, stearic acid, citric acid, and Hap) by extrusion under the same processing conditions used for the pure TPS:Ur blend. The samples were named as TPS:Ur/Hap 1:1, TPS:Ur/Hap 2:1 and TPS:Ur/Hap 4:1, respectively.

Characterizations

Dynamic light scattering

Dynamic light scattering (DLS) analyses were carried out on a High Performance Particle ZetaSizer (Malvern Instruments) to obtain the average particle sizes. 1mg of Ur/Hap nanocomposite sample was transferred to a 25ml glass bottle, which contained 10ml of distilled water. Before the DLS measurements, the solution was sonicated (Bransom 450 W) for 10min in order to disperse the Hap particles within the solution. For the TPS-based nanocomposites, the samples were kept in liquid nitrogen until complete freezing, and then ground with the aid of a mortar and pestle. About 1mg of sample powder was placed into 10ml of acetone and sonicated under equal conditions prior to the DLS measurements.

X-ray diffraction

A Shimadzu XRD6000 diffractometer was used to conduct X-ray diffraction analyses (XRD) of the nanocomposites. The relative intensity was registered in a diffraction range (2θ) of 3-40°, using a Cu-Kα incident beam (λ=0.1546 nm). The scanning speed was 1°min-1, the voltage and current of the X-ray tube were 30 kV and 30 mA, respectively.

Scanning electron microscopy

The morphology of the samples was analyzed by means of scanning electron microscopy (SEM) using a JEOL microscope model JSM 6510. The samples were dispersed over a carbon tape pasted on the surface of a metallic disc (stub). Then, the disc was coated with carbon in a Leica EM SCD050 chamber and imaged using the secondary electron mode.

X-ray Computed Micro-tomography

A pellet of each sample was placed in a rotating steel support and analyzed on a micro-tomography scanner (model 1172, SkyScan). The image acquisition process was conducted using the following parameters: unfiltered, spatial resolution (voxel size) of 2μm, 0.3° step rotation, 180° rotation and 6 frames for average process (averaging).The image reconstruction process of the tomographic sections was done by using the NRecon software (SkyScan) in which the following parameters were used: smoothing -5; ring artifact correction -5, and beam hardening correction of 60%.

Solubility Test

Phosphate release rate in acid solution

The determination of phosphorus was based on the method reported by Murphy and Riley,[14] which consists of an acidified solution of ammonium molybdate (Synth, Diadema, SP, Brazil) containing ascorbic acid (Synth, Diadema, SP, Brazil)and a small amount of antimony, which causes the formation and reduction of phosphomolybdic acid. The maximum absorption of the phosphomolybdenum blue formed in the presence of antimony occurs at a wavelength of 880 nm. Thus, an apparatus was arranged by placing a known mass of each sample inside dialysis membranes (Sigma-Aldrich, St. Louis, MO, USA)with dimensions of 15cm x 7.5cm which were immersed into citric acid solution 2% ($w.w^{-1}$), incubated and kept in a chamber at controlled temperature of 25°C (347 Fanem CD). Aliquot parts were collected at different time intervals up to 144hours. The phosphate quantifications were performed in triplicate. Concomitantly, it was also performed a test using only pure hydroxyapatite as a control experiment.

Urea release rate in acid solution

Urea solubilization experiments were performed simultaneously with the phosphorus solubilization tests,

according to a method adapted from Tomaszewska and Jarosiewicz.[15] The concentration of urea in solution was determined by UV-Vis spectrophotometer (Shimadzu-1601PC).[16] Each measurement was done in triplicate under identical experimental conditions for each sample.

Results and discussion

X-ray diffraction (XRD) results for pure Hap and Ur, and their corresponding nanocomposites are shown in Figure 1. The XRD patterns of all Ur/Hap nanocomposites displayed peaks ascribed to the Hap nanoparticles.[17] It can be seen the presence of a peak at 11° of 2θ in the pure Hap pattern which is related to the Hap lamellar phase.[18-21] This peak was absent in the nanocomposite patterns probably due to intercalation of urea into the lamellar space of Hap. As showed by Zuo et al.[19], the intercalation with DNA resulted in a remarkable reduction of this peak, with some displacement. This strategy is the same used to analyze polymerclay nanocomposites, where the (001) space in clay is analyzed through XRD.[22,23]

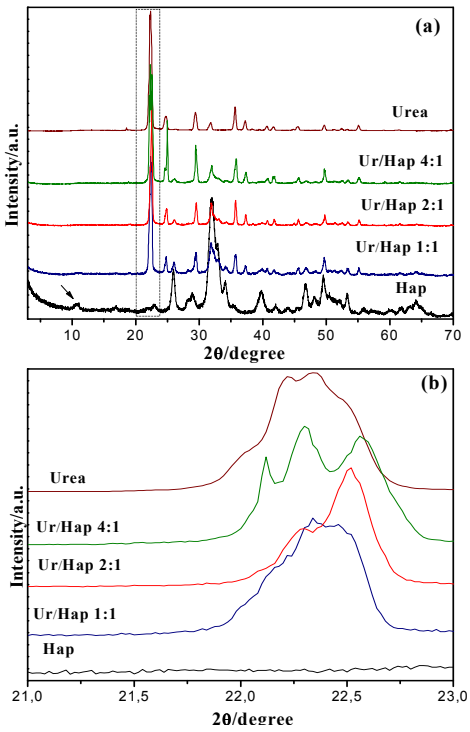

Figure 1. (a) XRD patterns of pure Hap, pure Urea and Ur/Hap nanocomposites; (b) expanded region of the peak at 22° relating to urea in the Ur/Hap nanocomposites.

The XRD pattern of pure Ur exhibited a set of peaks at 23, 25, 29, 32, 36, 37° of 2θ, which were still present, even showing lower intensity, in the XRD patterns of the nanocomposites. The decrease of the urea peak intensity can be explained by the chemical interactions between Ur and Hap as previously reported by Kottegoda et al.[24] The further analysis of the peak at 22° of 2θ strongly indicates the breakdown of the urea crystalline structure due to strong interactions with the Hap nanoparticles (Figure 1b). Then, one can expect that the XRD patterns, as well as other characterizations, are very influenced by this urea domains, which have the same features of pristine urea. Since the patterns reveal some small modifications in peak at 22-22.5°, this notices that the urea crystallization process was affected by Hap addition, but probably only in the interfaces. In Ur/Hap 4:1, better Hap dispersion probably affected by the higher interface area, as seen by the relative Hap size (as seen in Figure 3). In Ur/Hap 1:1, Hap agglomeration indicated lower interface areas, which is consistent to the other characterizations.

Scanning electron microscopy (SEM) was applied to characterize the morphology of the pure Hap and Ur/Hap nanocomposites (Figure 2).

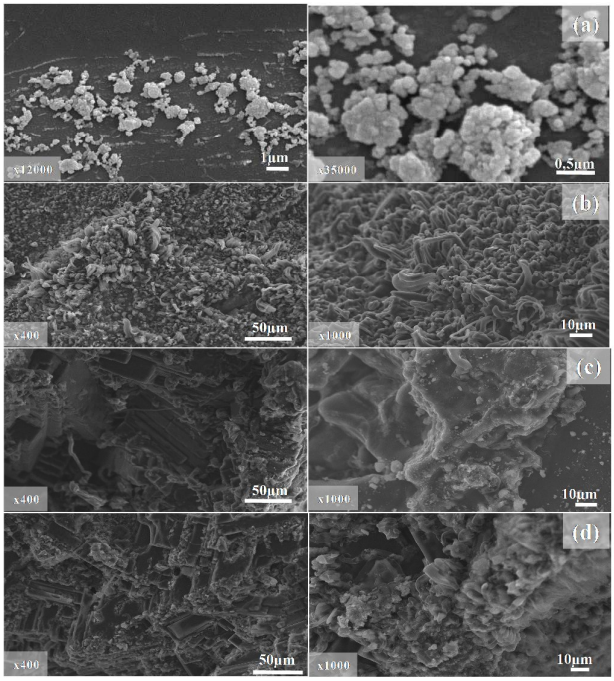

Figure 2. SEM images of (a) pure Hap and the Ur/Hap nanocomposites (b) Ur/ Hap 1:1, (c) Ur/Hap 2:1, and (d) Ur/Hap 4:1.

The Hap nanoparticles (Figure 2a were seen as solid agglomerates of very small nanoparticles (smaller than 100 nm) with atypical round-like morphology. The morphology of the Hap nanoparticles remarkably changed for each nanocomposite sample (Figure 2b-d), which may be a result of the urea intercalation process as observed by Pereira et al.[1324] In fact, the best dispersed structure was observed for the Ur/Hap 4:1 nanocomposite sample, which consisted of Hap nanoparticles separated by large domains of Ur. The Ur domains was found to be crystallized in the nanocomposite structure which supports the hypothesis that urea acted as a host matrix for the Hap nanoparticles. These results are concordance with the more intense Ur peaks in the Ur/Hap nanocomposites observed by XRD (Figure 1).

The phosphate solubility could be potentially increased by diminishing the size of its particles or by improving the dispersion of the particles, since the particle solubility of the particles depends on its size.[25] Since mineral phosphates have low solubility in water, turning them into very well dispersed small particles could promote an increase of surface area to interface the soil, consequently increasing the phosphate release rate. Complete solubilization of Ur was observed when the Ur/Hap nanocomposites were immersed into water, finely dispersing the Hap nanoparticles to the aqueous medium. Accordingly, it was possible to verify the influence of the Hap agglomeration concerning the different degrees of dispersion of the Hap nanoparticles within the nanocomposites matrix.

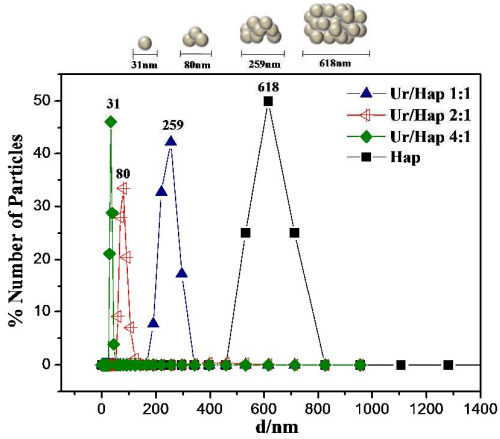

Figure 3. Influence of the Ur content on the Hap particle size. The scheme shows the state of aggregation of the Hap nanoparticles in the Ur/Hap nanocomposites.

The size of the Hap nanoparticles was determined by DLS for all nanocomposites samples after dissolution in water (Figure 3). It can be observed that the original agglomerates in pure Hap exhibited an average size of 618 nm. This is the largest size of agglomerates of Hap nanoparticles that could be found in the nanocomposite samples, as earlier observed by SEM (Figure 2). It was also suggested by SEM that the Ur matrix was able to reduce the Hap agglomeration because of the dispersion and immobilization of the Hap nanoparticles over its surface. DLS measurements further confirms this observation as the average Hap particle sizes for the nanocomposite samples Ur/Hap 1:1, Ur/Hap 2:1 and Ur/Hap 4:1 were found to be 249, 80, and 31 nm, respectively. Thus, the size of the Hap nanoparticles may be directly related to the content of Ur in the Ur/Hap nanocomposites, that is, the larger the urea content the smaller the Hap nanoparticles size. Possibly, the Hap nanoparticles were separated from each other by the continuous Ur domains, which ultimately prevented re-agglomeration of Hap in the nanocomposite, as illustrated in the scheme of Figure 3.

Figure 4a shows the phosphate release trend for the produced Ur/Hap nanocomposites in comparison with pure Hap. It can be noted that pure Hap has a low solubilization rate in acid medium, reaching only 37 % of solubilized phosphate over 144 hours. By analyzing the nanocomposite behavior, it may be noted that all formulations showed higher phosphate release rates compared with pure Hap, for example 60 % for Ur/Hap 4:1. A particular aspect is the kinetics observed for each system. It can be observed that there was a clear correlation between the agglomeration degree of the Hap nanoparticles and the percentage of released phosphate. The sample with smallest Hap particle size (Ur/Hap 4:1) exhibited the highest phosphate solubilization extent (100%). This result was clearly followed in extent by those found for the Ur/Hap 2:1 and Ur/Hap 1:1 nanocomposite samples, which displayed Hap particles sizes gradually larger, and consequently released 70 % and 50 %, respectively, of their total phosphate content.

The use of urea as a host matrix for Hap was interesting because of its high solubility in water and high commercial importance in agriculture. Thus urea release tests were also done for the Ur/Hap nanocomposites, as depicted in Figure 4b. The total dissolution of pure Ur occurred within 3 hours due to the saturation of the solution around the urea granule surface.

However, one can notice that all nanocomposite samples presented a delayed urea solubilization of up to 144 hours. It may be suggested that the interfacial chemical interactions between Ur and Hap (urea adsorption) are responsible for the delayed dissolution of the Ur matrix, considering the fact that urea was not totally free to react with water.

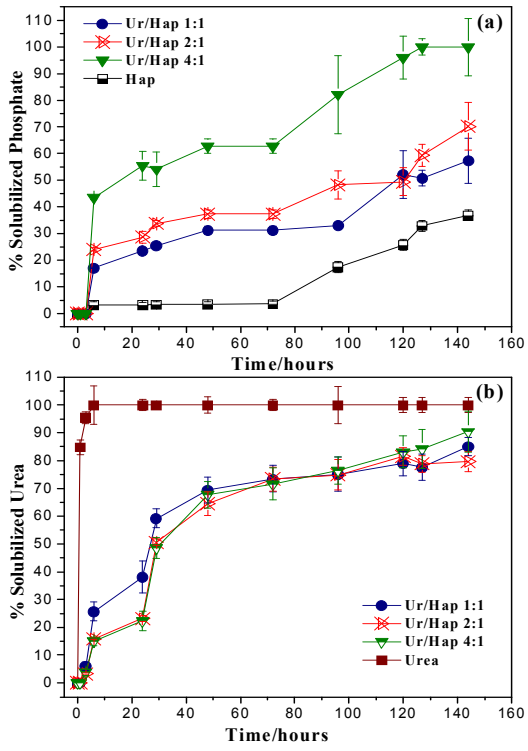

Figure 4. Solubilization rate of phosphate and urea as a function of time for pure Hap, pure Ur and Ur/Hap nanocomposites. Tests were done at pH 2 and temperature of 25 °C.

It is worth mentioning that the urea dissolution tests (complete immersion) were performed under very aggressive conditions. Even so the Ur release rates were comparable to

values found for other controlled release systems designed with basis on different concepts, as observed by Wu and Liu[26] for polymeric coatings in NPK granules. This denotes that the values found for the Ur/Hap are promising. In conventional application conditions, the samples would be exposed to low water contents, and one can expect a better urea retention effect for the Ur/Hap nanocomposites.

In order to analyze the influence of the matrix solubility on the phosphate release rate, similar amounts of Hap were dispersed in a TPS:Ur blend matrix. Figure 5 shows the XRD patterns of the pure components (TPS, Hap, Ur) and TPS:Ur/Hap nanocomposites containing different contents of Hap.

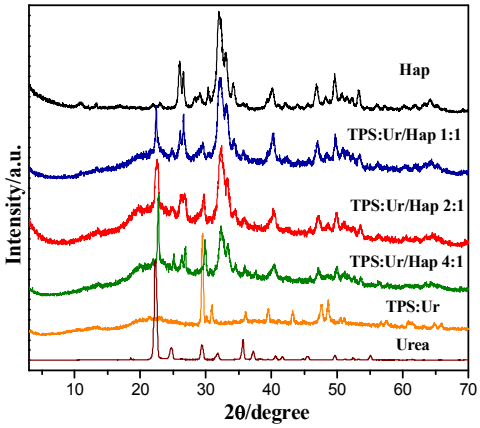

Figure 5. XRD patterns of Hap, pure TPS:Ur blend and nanocomposites TPS:Ur/Hap 1:1, TPS:Ur/Hap 2:1, and TPS:Ur/Hap 4:1.

Peaks associated with the granular native starch were not observed in the XRD pattern of the pure TPS:Ur blend, indicating that the extrusion process successfully produced a continuous matrix. Only peaks related to the presence of urea crystals can be seen in the XRD pattern of the pure blend. Furthermore, peaks related to the presence of Ur and Hap were notice able in the XRD patterns of the TPS:Ur/Hap nanocomposites. There was also a halo between 5 and 20° of 2θ which is related to the amorphous TPS portion of the nanocomposites. It is also observed a peak at approximately 22° of 2θ which can be ascribed to the presence of free urea domains in the polymeric network of TPS.[27]

Figure 6 shows SEM images of pure TPS:Ur and TPS:Ur/Hap nanocomposites. The complete disruption of starch is verified in Figure 6a by the occurrence of a continuous material with smoothed surface.[28] Large Ur crystals were not observed in the SEM image of the TPS:Ur blend, indicating that they were well embedded into the TPS structure. It was visibly observed that Hap played an important role on the TPS:Ur/Hap nanocomposite morphology evolution: all nanocomposites showed a porous architecture (Figure 6b-d), which is probably because of the release of moisture from starch during the extrusion process, generating structural voids controlled by the nanocomposite mechanical resistance – which is possibly related to different Hap amount. A good chemical compatibility between the TPS and Hap is suggested by the homogeneous phase material resulting from the mixture between TPS (matrix) and the Hap nanoparticles.

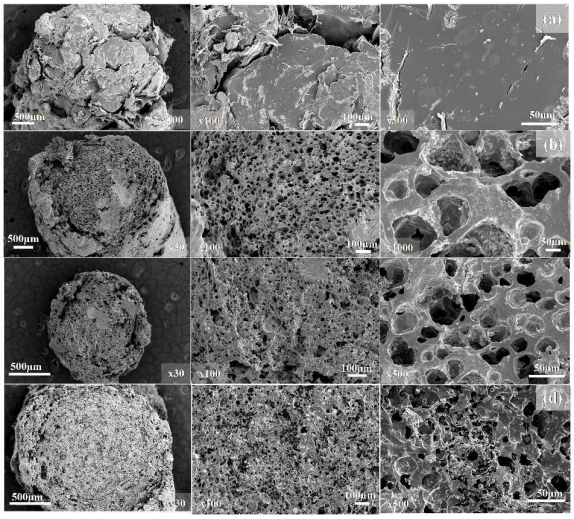

Figure 6. SEM images of (a) pure TPS:Ur and nanocomposites (b) TPS:Ur/Hap 1:1, (c) TPS:Ur/Hap 2:1, and (d) TPS:Ur/Hap 4:1.

In order to examine the porous structure of the TPS:Ur/Hap nanocomposites, a non-destructive X-ray tomography analysis was carried out. In this case, a full 3D image of internal structure of the samples was generated, which was useful to analyze the internal porosity resulting from the extrusion process.

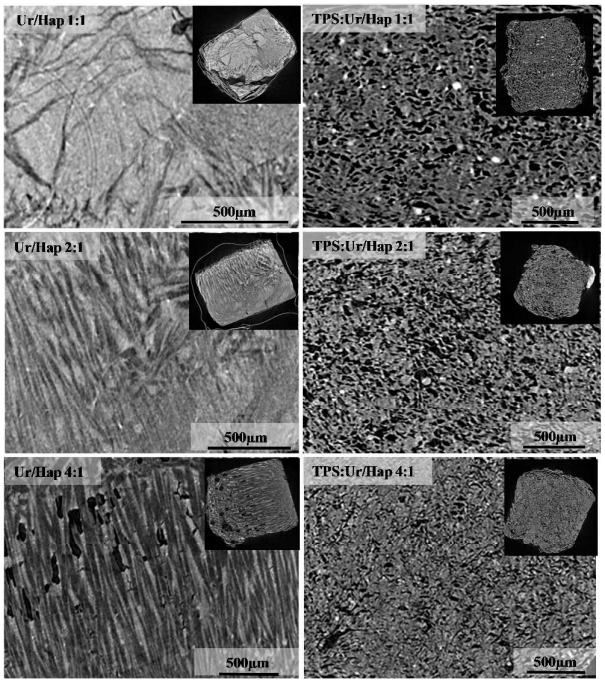

Figure 7. Cross-sectional images of the nanocomposites Ur/Hap and TPS:Ur/Hap/ obtained by X-ray micro-tomography.

Typical cross-sectional views shown in Figure 7 revealed that the presence of Hap was responsible for the formation of large porous in the structure of the TPS:Ur/Hap nanocomposites. The Ur/Hap nanocomposites were found to possess a dense microstructure, which was in accordance with the processing conditions used (Hap incorporation from melted urea). It is then expected that the large porosity of the TPS:Ur/Hap nanocomposites will facilitate the release of phosphate, since this will increase the total surface area accessible for dissolution. On the other hand, the compact structure of the Ur/Hap nanocomposites confirms that the Hap dissolution is driven by a previous dissolution of the Ur matrix.

Figure 8 displays the particle size distribution of Hap present in the TPS:Ur/Hap nanocomposite after complete dissolution in water. It is verified that the pure TPS:Ur matrix imparted a similar dispersion effect on Hap as that found in the case of the pure Ur host matrix. The Hap particle size decreased by approximately 85 % in comparison with pure Hap. There was no significant difference between the average size values found for the TPS:Ur/Hap nanocomposites. The result can be explained by re-agglomeration of small portions of Hap particles after dissolution of the nanocomposites, as illustrated by the drawing in Figure 8.

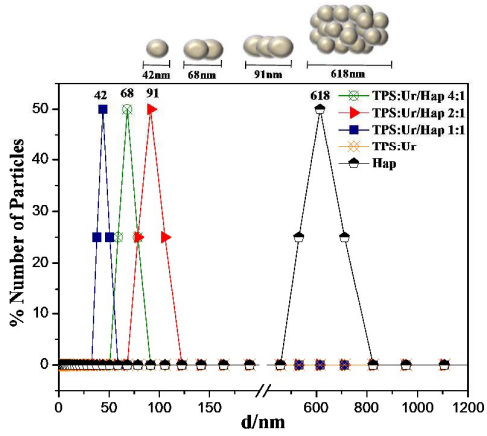

Figure 8. Distribution of Hap particle size of Hap occurring in the TPS:Ur/Hap nanocomposites.

The phosphate release evolution for the TPS:Ur/Hap nanocomposites in acid solution over time is presented in Figure 9a.All the TPS:Ur/Hap nanocomposites exhibited initial phosphate release faster than that observed for the Ur/Hap nanocomposites. The samples TPS:Ur/Hap 4:1, 2:1 and 1:1 presented phosphate release percentages of 90, 57 and 32 % after 24 hours, respectively. The largest phosphate percentage released both at initial and equilibrium point was noted for the nanocomposite containing the lowest content of Hap nanoparticles, probably due to the high hydrophilicity of the TPS:Ur matrix.

The different values found for the solubilization of phosphate are related to strong interactions between the TPS and Hap, and the high dispersion degree of the Hap nanoparticles within the TPS:Ur matrix. These interactions could have acted as a chemical barrier against the phosphate solubilization. It can also be observed that the TPS:Ur/Hap 1:1 sample presented a phosphate release similar to that of pure Hap. Furthermore, it is also noted the physical barrier effect imposed by the Hap nanoparticles, since the phosphate release rate was fully related to the swelling degree of the starch granules.

Urea release experiments were further conducted for the TPS:Ur/Hap nanocomposites (Figure 9b). All nanocomposites released Ur in a manner slower than the Ur solubilization. Additionally, it is verified that the nanocomposites containing high Hap contents presented a delayed urea release at same time, suggesting that the Hap nanoparticles acted as a physical barrier against the Ur solubilization.

A comparison between both types of nanocomposites developed in this study revealed that the TPS:Ur/Hap nanocomposites presented faster releases of phosphate and urea than the Ur/Hap nanocomposites, which are probably due to the water accessibility through their highly porous matrices.

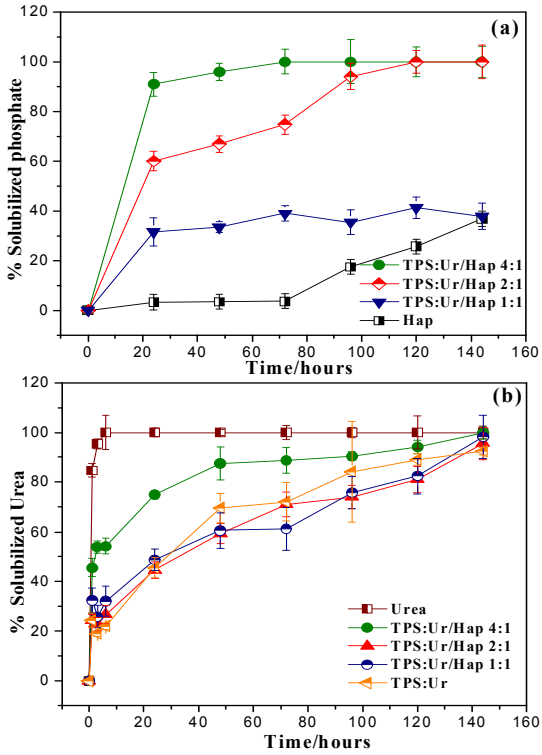

Figure 9. Phosphate solubilization rate (a) and urea solubilization rate (b) at 25 °C and pH2 as a function of time for pure Hap, pure Ur, and TPS:Ur/Hap nanocomposites.

Also, the TPS:Ur/Hap nanocomposites depicted a matrix less hydrosoluble and more rigid than Ur, meaning that the Hap nanoparticles were probably better isolated within their structure. Observing the release behaviors, one can notice different trends of diffusion between the Ur/Hap and TPS:Ur/Hap nanocomposites. A comparison between the phosphate release curves also allowed ascertaining which diffusion model driven the solubility of each nanocomposite. The release involves several mechanisms, including desorption

from the surface of the polymeric matrix, diffusion of the active compound through the pores of the polymer matrix or the polymer wall, the disintegration of the nanoparticles and subsequent release of the active compound, and dissolution and erosion of the matrix or wall. Table 1 shows the constant values obtained according to the equation proposed by Rigter and Peppas,[29] whose the kinetic parameter settings are given by Equation 1:

$$\frac{Mt}{Meq} = Kt^n \qquad (1)$$

where t is the time, K is the diffusion constant that depends on the type of material and the permeation medium, n is the difusional exponent which gives information about the type of transport mechanism for a given solute, and M_t and M_{eq} are the phosphorous concentration released at a time t and at the steady state, respectively. The parameter n values typically range from zero to one, where values of 0.5 correspond to a typical difusional release process and values of 1 means a zero order kinetic process. The n values greater than 1 indicate that the release is highly retained by a strong barrier, so that the total dissolution of the solute to the medium occurs at an infinite time.[30] Despite the Rigter and Peppas equation has been normally used to explain the slow/controlled release of molecules hosted by polymeric spheres, it can be used in the present case as an indicative of the real solubility of the Hap nanoparticles when shielded by the Ur and TPS:Ur matrices. In fact, since the solubilization is a difusional process, Equation 1 estimates the effect of the host matrix on the phosphate release.

Table 1. Kinetic parameters of phosphate release obtained by the Rigter and Peppas model.

Materials	*n*	*K* (s^{-1})
Hap	2.200±0.326	0.000689
Ur/Hap 4:1	0.3350±0.051	18.3707
Ur/Hap 2:1	0.4508±0.084	6.9374
Ur/Hap 1:1	0.4729±0.087	4.9760
TPS:Ur/Hap 4:1	0.0538±0.011	77.6700
TPS:Ur/Hap 2:1	0.3373±0.051	19.1463
TPS:Ur/Hap 1:1	0.1229±0.047	21.4819

The very low K value for pure Hap, along with the high n exponent is an indicative of low solubility of Hap under the experimental conditions. Despite the n value does not have a specific meaning, this can be interpreted as the high barrier for bare solubility in agglomerated powders, which was expected for Hap. For Ur/Hap nanocomposites, the n values approached 0.5, which indicates a classical diffusion mechanism, expected for freestanding nanoparticles (as proposed here). The K values were in accordance with the Hap content, i.e., higher Hap contents indicate lower release rates, as expected. On the other hand, the TPS:Ur/Hap nanocomposites showed much higher K values, which can be interpreted as a faster phosphate release when compared with the Ur/Hap nanocomposites. However, the lower n values (below 0.5 and without a clear tendency) show that the TPS played a role in prolonging the phosphate release time, which is probably associated with the swelling of the TPS:Ur matrix after some period of immersion into water. In fact, this is possible because the porous structure of the TPS:Ur/Hap nanocomposites can facilitate the release of phosphate at short times, but the structure is likely to be modified by swelling, obstructing the water transport over longer times. In this case, it is noticeable that the TPS:Ur/Hap 4:1 sample presented a n value close to zero, which is interpreted as a zero-order dissolution mechanism – close to that expected for very soluble phosphate sources.

Conclusions

In summary, our experiments showed the role played by the agglomeration of mineral phosphate powders on the effective solubilization of phosphate (i.e., phosphate release), demonstrating that it is possible to tailor a nanocomposite by finely dispersing hydroxyapatite (assumed here as a model for mineral phosphate fertilizers) within two matrices with different levels of hydrosolubility. The matrix solubility was found to be less important than the water accessibility in the nanocomposite structure, since the porous TPS:Ur matrix exhibited better phosphate release when compared with a dense urea matrix. However, it is important to notice that both types of host matrices are innovative, since TPS:Ur/Hap nanocomposites may provide a very fast phosphate release, whereas Ur/Hap nanocomposites enable an appropriate phosphate release with a delayed urea solubilization. The Hap-loaded nanocomposites are also interesting coupled fertilizers, since both components have nutritional effect in agricultural crops (i.e., as a source of P and N). These results could support the development of a new class of smart fertilizers, which can open new ways of applications for poorly soluble phosphate mineral phases.

Acknowledgements

This work was supported by FAPESP (São Paulo Research Foundation, Grant No. 2013/11821-5), CNPq and CAPES. We also acknowledge the Agronano Network (Embrapa Research Network) and National Nanotechnology Laboratory for Agribusiness (LNNA) for the institutional support and facilities.

Notes and references

1 M. N. A. Hasanaeen, H. M. M. Abdel-Aziz, D.M.A.El-Bialy, A. M. Omer, Afr. J. Biotechnol., 2014, **13,** 3158.
2 E. Corradini, M. R. de Moura, L.H.C. Mattoso, Express Polym. Lett., 2010, **4**, 509.
3 R. Liu, R. Lal, Sci. Total Environ., 2015, **514**, 131.
4 C.-Q. Xiao, R.-A. Chi, X.-H. Huang, W.-X. Zhang, G.-Z. Qiu, D.-Z. Wang, Ecol. Eng., 2008, **33**, 187.
5 M. C. de Rosa, C. Monreal, M. Schnitzer, R. Walsh, Y. Sultan, Nat. Nanotechnol., 2010, **5**, 91.
6 V. Mittal, O. Singh, H. Nayyar, J. Kaur, R. Tewari, Soil Biol. Biochem., 2008, **40,** 718.

7 A. M. Alston, K. W. Chin, J. Exp. Agric. Anim. Husb., 1974, **14**, 649.
8 F. Khasawneh, E. Doll, Adv. Agron., 1979, **30**, 159.
9 J. Watkinson, Soil Res.,1992, **32**, 1009.
10 D. Montalvo, M. J. McLaughlin, F. Degryse, Soil Sci. Soc. Am. J., 2015, **79**, 551.
11 R. Q. Liu, R. Lal, Sci. Rep., 2014, **4**, 5686.
12 D. Wang, S.A. Bradford, R.W. Harvey, B. Gao, L. Cang, D. Zhou, Environ. Sci. Technol., 2012, **46**, 2738.
13 E. I. Pereira, F. B. Minussi, C. C. T. da Cruz, A. C. C. Bernardi, C. Ribeiro, J. Agr. Food Chem., 2012, **60,** 5267.
14 J. Murphy, J. P. Riley, Anal. Chim. Acta,1962, **27**, 31.
15 M. Tomaszewwska, A. Jarosiewicz, J. Agric. Food Chem., 2002, **50**, 4634.
16 T. K. With, T. D. Petersen, B. Petersen, J. Clin. Pathol., 1961, **14**, 202.
17 C.-C. Wu, S.-T. Huang, T.-W. Tseng, Q.-L. Rao, H.-C. Lin, J. Mol. Struct., 2010, **979**, 72.
18 M. Sadat-Shojai, M.-T. Khorasani, A. Jamshidi, J. Cryst. Growth, 2012, **361**, 73.
19 G. Zuo, Y. Wan, X. Meng, Q. Zhao, K. Ren, S. Jia, J. Wang, Mater. Chem. Phys., 2011, **126**, 470.
20 F. Ye, H. Guo, H. Zhang, Nanotechnology, 2008, **19**, 245605, 7p.
21 G. Zuo, C. Liu, H. Luo, F. He, H. Liang, J. Wang, Y. Wan, J. Appl. Polym. Sci., 2009, **113**, 3089.
22 A. Giroto, A. de Campos, E. I. Pereira, T. S. Ribeiro, J. M. Marconcini, C. Ribeiro, React Funct Polym, 2015, **93**, 156-162.
23 A. Giroto, A. de Campos, E. I. Pereira, C. C. T. Cruz, J. M. Marconcini, C. Ribeiro J. Appl. Polym. Sci., 2014, **131**, 41188.
24 N. Kottegoda, I. Munaweera, N. Madusanka, V. Karunaratne, Curr. Sci., 2011, **101**, 73.
25 B. van Raij, Piracicaba: Ceres, 1991, 180.
26 L. Wu, M. Liu, Carbohyd. Polym., 2008, **72**, 240.
27 J.-L. Wang, F. Cheng, P.-X. Zhu, Carbohyd. Polym., 2014, **101**, 1109.
28 L. Averous, J. Macromol. Sci.-Polym. Rev., 2004, **44**, 231.
29 P.L. Ritger, N.A. Peppas, J. Control. Release, 1987, **5**, 26.
30 P.L. Ritger, N.A. Peppas, J. Control. Release, 1987, **5**, 37.

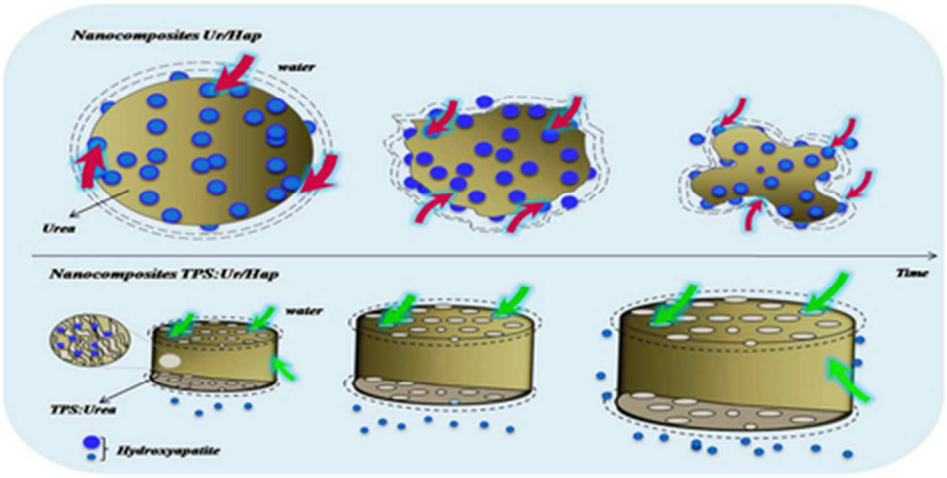

39x19mm (300 x 300 DPI)